RSC Advances

PAPER

View Article Online
View Journal | View Issue

Cite this: *RSC Adv.*, 2026, **16**, 28892

Synthesis and application of UV responsive detachable adhesives from epoxidized plant oils

Muhammad Hassan Ahmad,[a] Muhammad Atif *[a] and Bilal Anjum Ahmed[b]

Received 24th February 2026
Accepted 21st May 2026

DOI: 10.1039/d6ra01625a

rsc.li/rsc-advances

Permanent adhesives pose significant environmental concerns because they cannot be reversed or recycled, limiting repair, reuse, and material recovery. Temporary and reversible adhesives offer a better option by allowing removal, repair, and recycling when needed. In this study, UV-responsive adhesives were prepared from natural oils, including castor, sesame, mustard, and eucalyptus, without using a photoinitiator. Five formulations (UVad-1 to UVad-5) were developed and tested. Their physical, structural, and mechanical properties were evaluated. Samples containing sesame and castor oil (UVad-4) and samples with eucalyptus and mustard oil (UVad-5) exhibited superior detachment and reusability, achieving up to 10 and 12 cycles of bonding and debonding under 638.79 KN m^{-2} and 532.97 KN m^{-2} applied stress, respectively. Mechanical strength was also evaluated under UV and non-UV conditions. Results indicate that these materials are suitable for temporary yet robust bonding and reuse.

1 Introduction

Adhesives are substances used to attach two surfaces without mechanical fastening.[1,2] They bond by physical or chemical contact.[3] Adhesives are generally classified as permanent or removable. Permanent adhesives are long-lasting and difficult to remove,[4] whereas removable adhesives permit controlled separation when needed.[5] Adhesives can also be classified by chemistry, curing mechanism, or responsiveness to external stimuli.[6] Adhesives find diverse applications across fields such as electronics,[7] automotive manufacturing,[8] construction, packaging,[9] and biomedical products.[10] They offer advantages over mechanical fastening, including uniform stress distribution, light weight, design flexibility, and compatibility with complex or delicate surfaces.[11] Adhesive bonding also promotes miniaturisation and eliminates the need for drilling, welding, or thermal processing.[5] Nonetheless, most traditional adhesives form permanent bonds that are hard to break. This poses issues for repairing, recycling, and dismantling, and can result in material waste, damage, residue, and waste production.[12]

Increased demand for reuse, repair, and recycling has enhanced focus and research about detachable adhesives.[13,14] These materials form strong bonds during use and can be released upon external stimulation.[15–17] They respond to heat, pH, moisture, pressure, ultrasound, electricity, magnetism, or light. Nevertheless, both types are associated with weaknesses, including damage to sensitive components, potential for residue in pH-sensitive systems, softening of moisture-sensitive adhesives on soft surfaces, and use of pressure-based systems.[5,18–22] Safety and compatibility may also be issues with ultrasonic, electrical, and magnetic methods.[4,8,23–32] Such limitations point to the need for cleaner and more selective reversible bonding methods.

UV light can be used as an accurate and non-contact method for adhesive detachment. UV-based separable systems can be separated without the use of heat, chemicals, or mechanical force, which is beneficial for protecting valuable resources.[33–36] When bio-based sources are used to create UV-responsive adhesives, these materials eliminate the use of synthetic materials and support the sustainability purpose.[37] These systems enable clean removal, controlled activation, and minimal residue. Their selective response makes them suitable for applications where surface preservation and recyclability are important.[38,39]

Several studies have reported UV-responsive detachable adhesives based on synthetic photoinitiators. Kim *et. al.*,[13] formulated UV-responsive detachable optically cleared acrylic adhesives (OCA) using benzophenone-derived initiators that detached under 365 nm UV at 4200 mJ cm^{-2}, but sometimes left residue and needed an addition of an external photoinitiator. Wang *et. al.*,[14] developed coumarin-based pressure-sensitive tapes with peel strength up to 10.15 N cm^{-1} and reversible adhesion under 254 nm and 365 nm UV. This formulation lacks an intrinsic photoinitiator capability and relies on the addition of a coumarin-based photoinitiator. Another study by Kim *et. al.*,[40] used nitrobenzyl dimethacrylate and observed a drop in adhesion from 341 kPa to 223 kPa, a reduction of 38% after 30 min irradiation, and further decreased to 150 kPa after 3 h, resulting in a total drop of 56%. These systems demonstrate UV-

[a]*Chemistry Department, University of Education Lahore (Vehari Campus), Punjab, Pakistan. E-mail: muhammad.atif@ue.edu.pk; chemistatif@yahoo.com*

[b]*Core Research Facilities, Research Institute, King Fahad University of Petroleum and Minerals, Dhahran, Saudi Arabia*

Table 1 Literature review of UV-responsive detachable adhesives

Starting materials	Catalyst	Substrate	DB UV (nm)/ Intensity ($mWcm^{-2}$)	PI	DB time/cycles	Product	Ref.
nBA, HBA, BA, DMAEA, DMAEAc	Cyanoarene	Glass	365/14	4Cz-IPN	5 min/NR	OCA	13
HMC, HEOMC, PPG1000, 2-HEA, IPDI	DBTDL	Glass	365/31.3	Coumarin	5 min/NR	S-PSA	14
pSBMA, DOPA, dioxane, $KMnO_4$	AIBN	Polyester	352/NR	NBDM	3.5 h/5	MDOPA-*co*-SBMA-*co*-NBDM	40
EuO, HEuO, MSO, HMSO, HSSO, CaO, DMG, glycerin, TDI	DBTDL	Glass	365/20	Nil	3 min 47 s/4 23 s/10 43 s/12	UVad-2 UVad-4 UVad-5	[a]

[a] This work, NR = not reported; *n*BA = *n*-butyl acrylate; HBA = d 4-hydroxybutyl acrylate; DMAEA = dimethylaminoethyl acrylate; DMAEAc = dimethylaminoethyl acetate; 4Cz-IPN = 2,4,5,6-tetra(9H-carbazol-9-yl)isophthalonitrile; OCA = optically clear adhesive; HMC = 7-hydroxy-4-methylcoumarin; HEOMC= (7-hydroxy-ethoxy-4-methylcoumarin); PPG1000 = polypropylene glycol; 2-HEA = hydroxyethyl acrylate; IPDI = isophorone diisocyanate; S-PSA = switchable pressure sensitive adhesives; pSBMA = poly(sulfobetaine methacrylate); DOPA = 3,4-dihydroxyphenylalanine; NBDM = 2-nitro-1,3-benzenedimethanol dimethacrylate; AIBN = azobisisobutyronitrile; MDOPA-*co*-SBMA-*co*-poly(*N*-methacryloyl-3,4-dihydroxyl-L-phenylalanine-*co*-sulfobetaine methacrylate-*co*-2-nitro-1,3-benzenedimethanol dimethacrylate; EuO = eucalyptus oil; HEuO = hydroxylated eucalyptus oil; MSO = mustard seed oil; HMSO = hydroxylated mustard seed oil; HSSO = hydroxylated sesame seed oil; CaO = castor oil; DMG = dimethyl glyoxime; TDI = toulene 2-4,diisocyanate; DBTDL = dibutyl tin dilaurate.

triggered detachment but still face limitations such as surface residue, reduced strength over time, and dependence on synthetic photoinitiators (Table 1).

This study presents a new type of UV-responsive Polyurethane (PU) adhesive made entirely from plant oils, without using synthetic photoinitiators. Oils such as Castor (CaO), Mustard seed (MSO), Sesame seed (SSO), and Eucalyptus (EuO) were used for their natural response to UV light. Adhesives exhibited good bonding under normal conditions and easy detachment when exposed to UV light. They also performed well in terms of mechanical strength, water resistance, thermal stability, and repeated attachment–detachment cycles. By replacing petrochemical ingredients with renewable materials, this work supports the development of practical and eco-friendly adhesives for modern applications.

2 Experimental

2.1 Materials

EuO, MSO, SSO, and CaO were purchased from the local market. Dimethyl glyoxime (DMG) (1.37 g cm^{-3}) was purchased from Simpsons. Toluene 2,4-diisocyanate (TDI) (1.21 g cm^{-3}) was purchased from DAEJUNG. Dichloromethane (DCM, ≥99%), hydrogen peroxide (35%), formic acid, acetic acid, and ethanol were purchased from Sigma. Dibutyl tin dilaurate (DBTDL, catalyst) was purchased from Fluka Chemika. All chemicals were utilised as received, without purification.

2.2 Sample preparation

Sample preparation was carried out in two steps. The first step involved modifying plant oils, and the second step involved adhesive preparation using unmodified and modified plant oils.

2.2.1 Plant oil modification. Three plant oils (EuO, SSO, and MSO) were modified *via* a two-step process: epoxidation and hydroxylation.

Epoxidation of EuO was performed according to the reported method.[41] 0.0073 mol acetic acid and 0.19 mol 35% H_2O_2 were condensed at 60 °C for 2.5 h with a dropwise addition of 0.06 mol EuO. Mixture was heated at 130 °C for 30 min, organic layer (Ep-EuO) was separated and used for hydroxylation.

For hydroxylation, 0.28 mol of deionised (DI) water, 0.133 mol formic acid, and 0.137 mol ethanol were heated at 60 °C with continuous stirring. Ep-EuO (0.026 mol) was added dropwise, and mixture was heated for 30 min. HEuO layer was separated after 24 h. SSO was epoxidised and hydroxylated using the same reported procedure. Similarly, MSO was also epoxidised and hydroxylated following the same reported procedure utilised for previous oil modifications.

2.2.2 Adhesive preparation. Five biobased UV-responsive PU adhesives have been prepared, as per the compositions given in Table 2. In general, selected plant oils were heated (50–60 °C) and mixed for homogenisation, followed by the addition of DMG with ethanol as solvent. DBTDL was introduced at 60–70 °C, and TDI was added dropwise under continuous stirring. Glycerin was incorporated at the final stage to adjust softness and flexibility. Mixtures were then cured under mild heating, depending on the formulation.

Small changes were made for some adhesives: UVad-3 used HEuO instead of EuO, UVad-2 had slightly more MSO to change gelation time, UVad-4 replaced EuO/MSO with CaO/HSSO, and UVad-1, UVad-3, and UVad-5 had slight differences in curing time.

3 Characterisation

Fourier Transform Infrared Spectroscopy (FTIR, IRSprit, Shimadzu) with diamond ATR was used to identify functional groups of prepared samples in the 400–4000 cm^{-1} range. Simultaneous Thermal Analysis (STA) (SKZ1060A Industrial Co.) was conducted with an aluminum crucible from 30 to 500 °C with a 10 °C min^{-1} ramp rate in N_2 for Thermogravimetric analysis (TGA), Differential Scanning Calorimetry (DSC), and

Table 2 UV-responsive adhesive composition

Sample	BioSource (mol)						DMG (mol)	Solvent (mol)	DBTDL (mol)	TDI (mol)	Glycerin (mol)	PU (wt%)
	EuO	HEuO	MSO	HMSO	CaO	HSSO						
UVad-1	6×10^{-3}	—	9.2×10^{-3}	—	—	—	6.9×10^{-3}	8.6×10^{-2}	8×10^{-3}	6.9×10^{-3}	6.8×10^{-3}	51.51
UVad-2	6×10^{-3}	—	4.6×10^{-3}	—	—	—	6.9×10^{-3}	8.6×10^{-2}	8×10^{-3}	6.9×10^{-3}	6.8×10^{-3}	58.82
UVad-3	—	5×10^{-3}	4.6×10^{-3}	—	—	—	6.9×10^{-3}	8.6×10^{-2}	8×10^{-3}	6.9×10^{-3}	6.8×10^{-3}	58.60
UVad-4	—	—	—	—	1×10^{-3}	8.2×10^{-4}	6.9×10^{-3}	8.6×10^{-2}	8×10^{-3}	6.9×10^{-3}	2×10^{-2}	49.54
UVad-5	1.2×10^{-2}	—	4.6×10^{-3}	2.6×10^{-3}	—	—	1.7×10^{-3}	3.4×10^{-2}	3.4×10^{-4}	3.4×10^{-3}	7.2×10^{-3}	21.57

Differential Thermal Analysis (DTA) of samples. Macrophasic imaging was taken by microscope (IRMECO GmbH & Co., IM-910) while nano-scale surface morphology was determined by FESEM (Tescan Lyura-3). Ebullioscopic method (eqn (1)) was used to determine the molar mass (MM) of unmodified and modified oils using benzene as a solvent.[42]

$$\Delta T_b = K_b m \quad (1)$$

ΔT_b is elevation in solvent's boiling point, K_b is ebullioscopic constant, and m is sample's molality. K_b for benzene is 2.53 °C kg mol^{-1}.[41]

A slightly modified reported method has been used to determine iodine value (IV).[42] A sample of 0.2 g in 10 mL of chloroform was mixed with 30 mL of Hanus solution for 30 min. A 10 mL aliquot of 15% KI solution was diluted with 100 mL of DI and subsequently titrated with 0.1 N $Na_2S_2O_3$ until a yellow color endpoint was reached. 2 drops of indicator were added, and titration proceeded until a blue color appeared. IV was calculated by using eqn (2).

$$\mathrm{IV} = \frac{(B-S)\cdot \mathrm{N\ of\ Na_2S_2O_3}\cdot 0.127\mathrm{g/meq}\cdot 100}{\mathrm{Weight\ of\ Sample(g)}} \quad (2)$$

Here, B and S represent volume of $Na_2S_2O_3$ applied to blank and sample solutions, respectively, while N represents normality of $Na_2S_2O_3$.

HCl-acetone titration-based method[42] has been used to determine epoxy value (EV). A sample solution was prepared by mixing 0.25 g of sample in 5 mL of HCl (0.1 N) and 35 mL of acetone. 5 mL of this solution with 2 drops of indicator was titrated with 0.1 N NaOH until the pink color endpoint was reached. EV was calculated by eqn (3).

$$\mathrm{EV} = \frac{(B-S)\cdot \mathrm{N\ of\ HCl}}{W \times 10} \quad (3)$$

S and B denote volume of NaOH used for sample and blank solutions, respectively, while W denotes weight of the sample.

Free fatty acid (FFA) was determined by using a reported method of acid-base titration.[43] 1.5 g of oil was dissolved in 25 mL of ethanol, and after the addition of 2 drops of phenolphthalein, solution was titrated with 0.1 N NaOH until a pink hue emerged. Determination of FFA was conducted through the application of eqn (4).

$$\mathrm{FFA} = \frac{V \times N \times M}{W \times 1000} \quad (4)$$

where V is volume of NaOH used, N is normality of NaOH, M is molar mass of oil, and W is weight of oil taken.

Samples' water absorption capacity (WAC) was determined using a previously reported method.[4] Weighed adhesive samples were immersed in DI water for specified time intervals of 1, 2, 3, 4, 24, 48 h and 72 h. Samples were promptly taken out of water and subsequently dried to determine their WAC through the application of eqn (5).

$$\mathrm{WAC}(\%) = \frac{W_t - W_o}{W_o} \times 100 \quad (5)$$

In eqn (5), W_o denotes weight of dry sample, while W_t indicates weight of sample after soaking.

Gel content (GC) was evaluated in samples using a reported method.[4] % GC in adhesive was calculated by immersing a weighed amount of adhesive in 10 mL of DCM for 24 h. Subsequently, samples were taken out from solvent and allowed to dry at ambient temperature, and samples were weighed again. Eqn (6) and (7) were used to estimate GC of samples.[18]

$$\%\ \mathrm{Extract} = \frac{W_s - W_d}{W_s} \times 100 \quad (6)$$

$$\%\ \mathrm{GC} = 100 - \%\ \mathrm{Extract} \quad (7)$$

W_s and W_d represent sample weights before and after soaking, respectively.

PU weight percent content of prepared adhesives (% wt PU) was calculated by using eqn (8).

$$\%\ \mathrm{weight\ of\ PU} = \frac{M_{TDI} - M_{DMG}}{M_{TDI} - \mathsf{M}_{oil} - M_{DMG}} \times 100 \quad (8)$$

Mechanical evaluation of UV-responsive adhesive samples (UVad-1 to UVad-5) was performed using single lap joint (SLJ) method, following the reported methods outlined in literature, while standardised methods such as ASTM D1002 are typically conducted on universal testing machines, this study employed a custom-built dead-weight loading apparatus to evaluate the apparent shear strength of SLJ. This simpler and cost-effective approach is supported by prior research, which highlights the validity of using non-standardised test setups for comparative adhesive assessments, particularly when access to advanced instrumentation is limited.[4,6,44] Two clean glass slides (25 × 75 mm^2) were used as adherends, and 0.08 g of adhesive was applied uniformly to a defined overlap area. Slides were gently

pressed together to ensure even spreading of adhesive and were allowed to cure at room temperature for about 1 hour. After curing, bonded joints were subjected to weight-bearing tests where known weights were gradually applied to bonded slides until joint failure occurred, and the maximum load sustained before failure was recorded. Strength of bonds was then calculated as normalised applied load relative to effective bonded area, allowing comparison across all samples and several reattachments.

Normalised force (F_N) was determined by eqn (9).[4] Applied pressure was calculated by taking force (N) and dividing it by the area of the adhesive (m^2).

$$F_N = \frac{P - p_{min}}{p_{max} - p_{min}} \quad (9)$$

Statistical analysis for cycle-to-cycle change, like mean, standard deviation (SD), and Coefficient of variation (CV), was evaluated by using eqn (10)–(12), respectively.

$$\text{Mean} = \frac{\text{Number of values}}{\text{Sum of all values}} \quad (10)$$

$$\text{SD} = \sqrt{\frac{\sum (x - \bar{x})^2}{n - 1}} \quad (11)$$

Here, x = each value in the data set, $\bar{x}$ = the mean (average) of all values, and n = total number of values.

$$\text{CV} = \frac{\text{SD}}{\text{Mean}} \times 100 \quad (12)$$

4 Results and discussion

4.1 Oil analysis

Plant oils were comprehensively characterised *via* physico-chemical and instrumental analysis, both prior to and following chemical modification.

4.1.1 Physico-chemical analyses. Molecular mass (MM), IV, EV, density, and FFA of both unmodified and modified oils were calculated (Table 3) to check the efficacy of modification method. Increase in MM and density of modified oils, compared to their unmodified counterparts, proves a transformation in molecular structure. IV difference proved the efficient utilisation of unsaturated components during two-step modification process of plant oils. EV has been validated as a good indicator for epoxidation of plant oils. Ep-EuO showed a increase in EV, confirming successful epoxidation, while IV of EuO decreased from 123.6 to 70.5 (g I_2/100 g), indicating a decrease in unsaturation degree.

4.1.2 FTIR. A comparative FTIR analysis (Fig. 1) of both unmodified and modified oils was done to elucidate progressive two-step chemical modifications. FTIR spectra of EuO (Fig. 1a) had two prominent peaks at 1140 cm^{-1} (C–O–C) and 2900 cm^{-1} (C–H str).[45] After the first step of modification, peaks at 826 cm^{-1} (ref. 42) were obtained in Ep-EuO, supporting the formation of epoxy. By end of the modification of second step, HEuO had an increase of hydroxyl groups at 3400 cm^{-1},[46] indicating successful hydroxylation. FTIR spectra of SSO, ESSO, and HSSO (Fig. 1b) showed presence of prominent chemical changes where SSO showed distinct C=C–H str peaks at 3008 cm^{-1},[41] along with C–O–C linkages at 1242 cm^{-1}.[41] Epoxidation was verified by presence of peak reduction for C=C (723 cm^{-1})[41] and =C–H bend (3008 cm^{-1}),[41] as well as epoxy peak appearance at 826 cm^{-1}.[42] In addition, widening of the C–O–C peak suggests an increase in ether linkages. After hydroxylation, O–H peak (3500 cm^{-1})[4] broadened, whereas C–O–C and epoxy peaks decreased, indicating the process of epoxy ring opening and later generation of hydroxyl groups.

FTIR spectra (Fig. 1c) of the transformation of MSO to EMSO and HMSO confirmed chemical transformation. MSO had characteristic peaks of hydrocarbons (3000 cm^{-1}),[47] C=C of alkene (1660 cm^{-1}),[48] and amide II band (1533 cm^{-1}) (*N*–H bending coupled with C–N stretching)[49] attributed to the presence of proteinaceous components in crude mustard oil. Epoxidation of MSO resulted in the appearance of new peaks at 1700 cm^{-1} (carbonyl group),[41] 1250 cm^{-1} (C–O–C stretching),[41] and 826 cm^{-1} (epoxy group),[42] indicating successful chemical modification. Hydroxylation gave another broad peak between 3400–3600 cm^{-1} (hydroxyl)[4] and at 1700 cm^{-1} (carbonyl),[41] showing a successful hydroxylation.

4.2 Adhesive analysis

Prepared adhesives were subjectively characterised using physicochemical and instrumental analysis to determine their

Table 3 Physico-chemical analysis data of unmodified and modified plant oils

Sample	MM (g mol^{-1})	IV (g I_2/100g)	EV (mmol g^{-1})	FFA (%)	Density (g cm^{-3})
EuO	154.25	123.6	3.2	0.073	0.9225
Ep_EuO	178.6	70.5	105.5	0.0809	0.9301
HEuO	185.2	61.8	93.5	0.0987	0.9351
SSO	1103.5	129.20	104.78	0.798	0.9140
ESSO	1290.1	114.25	131.15	1.03	0.9520
HSSO	1322.3	100.70	104.95	1.366	1.0881
MSO	99.15	104.20	1.75	0.008	0.912
EMSO	158.6	90.55	5.05	0.066	0.942
HMSO	189.16	7.88	2.31	0.055	0.975
CaO	933.43	95.25	5.6	0.099	0.9585

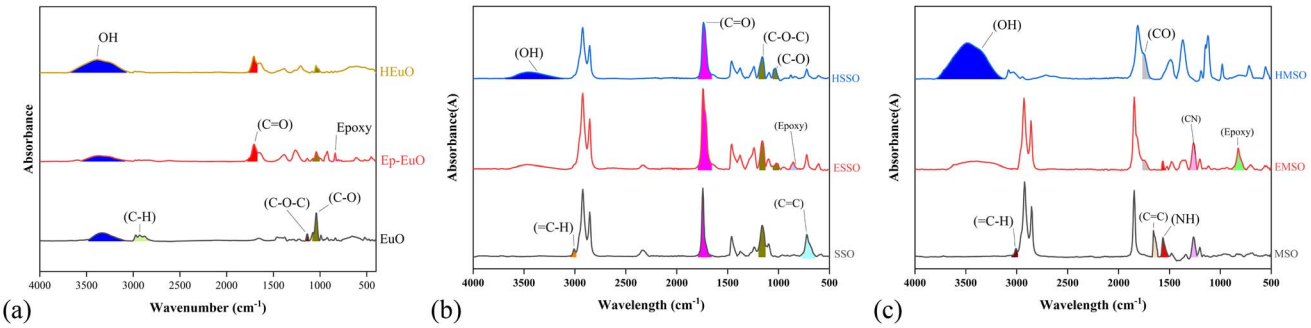

Fig. 1 FTIR spectra comparison for the modification of (a) EuO, (b) SSO, and (c) MSO.

chemical and structural characteristics. Additionally, their adhesive strength was compared using SLJ tests.[50–52]

4.2.1 FTIR. Ingredients of UVad-1 and UVad-2 (Fig. 2a and b) presented prominent peaks of OH str (at 3200–3400 cm^{-1}) from glycerin and DMG,[53] NCO str from TDI at 2245 cm^{-1},[41] and MSO unsaturation C=C peak at 1660 cm^{-1}.[48] Following the reaction completion, FTIR analysis of prepared adhesive revealed the disappearance of NCO peak, indicating utilisation of TDI isocyanate. Emergence of a C–N peak at 1230 cm^{-1} further substantiated the successful formation of adhesive. Moreover, a strong C=O str peak at 1700 cm^{-1} (ref. 41) and *N*–H str peak at 3300 cm^{-1} are characteristic peaks of urethane group. Further evidence has emerged from new peaks observed in the range of 1000–1200 cm^{-1}, specifically relating to C–O stretching,[4] which is a major component of PU adhesive network. A slight reduction in the C=C peak indicates partial utilisation of the functional group.

FTIR spectrum of UVad-3 showed the quenching of OH and NCO peaks, indicating consumption of these functional groups during synthesis. Concurrently, new peaks emerged at 1048 cm^{-1} (C–O), 3293 cm^{-1} (NH), and 1230 cm^{-1} (C–N), confirming the formation of urethane bonds.[41]

FTIR spectrum of UVad-4 exhibited characteristic peaks corresponding to OH groups from glycerin, DMG, and HSSO in range of 3200–3500 cm^{-1}.[4] Additionally, NCO group from TDI was observed at 2245 cm^{-1}.[41] Isocyanate groups reacted with hydroxyl groups to form urethane bonds, resulting in maximum consumption of NCO groups, as evidenced by the disappearance of NCO peak. FTIR analysis verified the formation of urethane groups, with characteristic peaks observed for C=O str at 1700 cm^{-1} (ref. 4) and *N*–H str at 3300 cm^{-1}.[41] Additionally, peaks at 1538 cm^{-1} indicated the presence of aromatic or cyclic structures,[41] while C–O str vibrations within 1100–1200 cm^{-1} range[4] further supported the development of a robust urethane network.

UVad-5 spectrum revealed OH str from Glycerin, DMG, and HMSO at 3200–3500 cm^{-1} (ref. 42) and TDI's NCO peak at 2245 cm^{-1}.[41] MSO and EuO C=C str at 1660 cm^{-1} indicated unsaturation.[48] Formation of adhesive was evidenced by the vanishing of NCO and OH peaks, signifying a successful

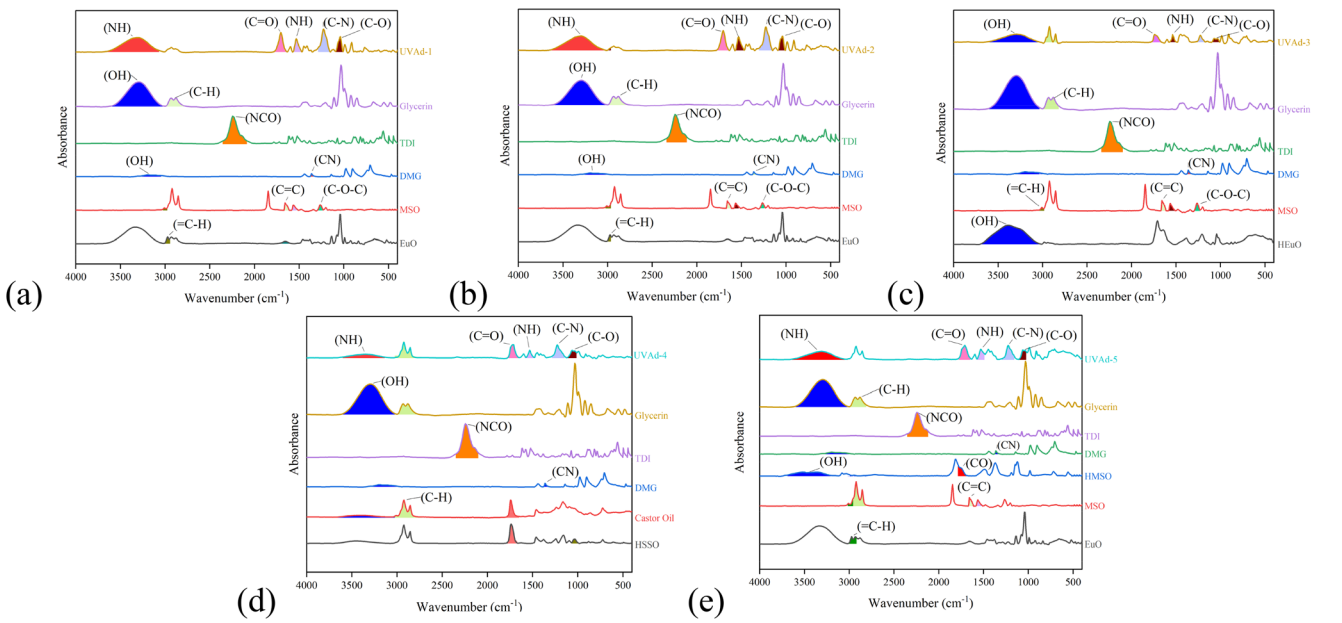

Fig. 2 FTIR of UVad-1 (a), UVad-2 (b), UVad-3 (c), UVad-4 (d), UVad-5 (e), and its components.

reaction between isocyanates and hydroxyls that created urethane bonds. Appearance of new peaks at approximately 1703 cm^{-1} (C═O)[41,42] and 3300 cm^{-1} (N–H)[41] indicated formation of urethane linkages. Reduction of the C═C peak at 1660 cm^{-1} suggested cross-linking in unsaturated oils. Urethane network was supported by C–O str at 1100–1200 cm^{-1},[4] while peaks at 1219 cm^{-1} (C–N) indicated production of PU linking after cross-linking.[4]

4.2.1.1 Proposed reaction mechanisms. The proposed mechanism was developed based on FTIR data (Section 4.3), taking into account the sequence of ingredient addition during sample preparation. Five adhesive samples with different formulations and PU content displayed varying UV-responsive detachment, load-bearing capacity, and reusability, revealing the influence of molecular structure and network connectivity on adhesive properties. A possible UV-induced detachment mechanism is suggested (Scheme 1), involving interactions between DMG and 1,8-cineole.

In samples UVad-2 and UVad-5, the presence of DMG's hydroxyl group in close proximity of 1,8-cineole may facilitate detachment, whereas absence of this situation in UVad-1 may explain the lack of responsiveness. In sample UVad-3, widespread cross-linking because of HEuO may limit DMG's bonding with 1,8-cineole, suppressing detachment. In sample UVad-4, DMG and CaO (natural PI) connections may contribute to UV-based detachment.

4.2.2 TGA and DTA. TGA spectra provided thermal degradation behavior of prepared adhesive samples, which has been marked by three distinct segments; *i.e.*, rt-150 °C, 151–300 °C, and 301–500 °C (Fig. 3). A slight weight loss was observed at start of TGA run, which could be associated with the evaporation of volatile components and residual moisture because of the presence of solvent and volatile components present in polyols in the formulations.[6,54] In particular, weight losses observed for UVad-1, UVad-2, UVad-3, UVad-4, and UVad-5 have been 11.66%, 11.23%, 7.63%, 10.01%, and 5.49%, respectively.

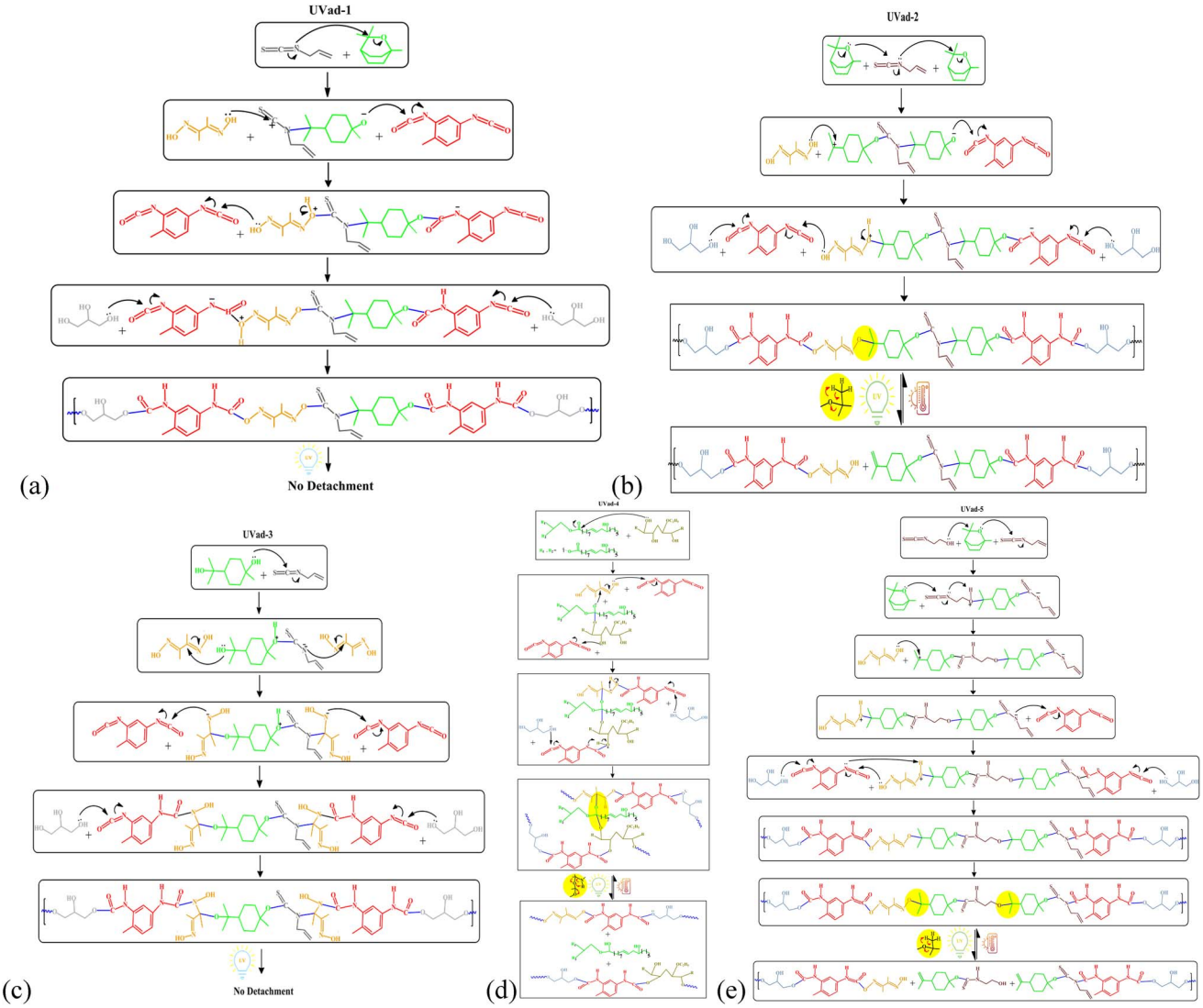

Scheme 1 Proposed mechanisms for synthesis and UV detachment of prepared samples as (a) UVad-1, (b) UVad-2, (c) UVad-3, (d) UVad-4, and (e) UVad-5.

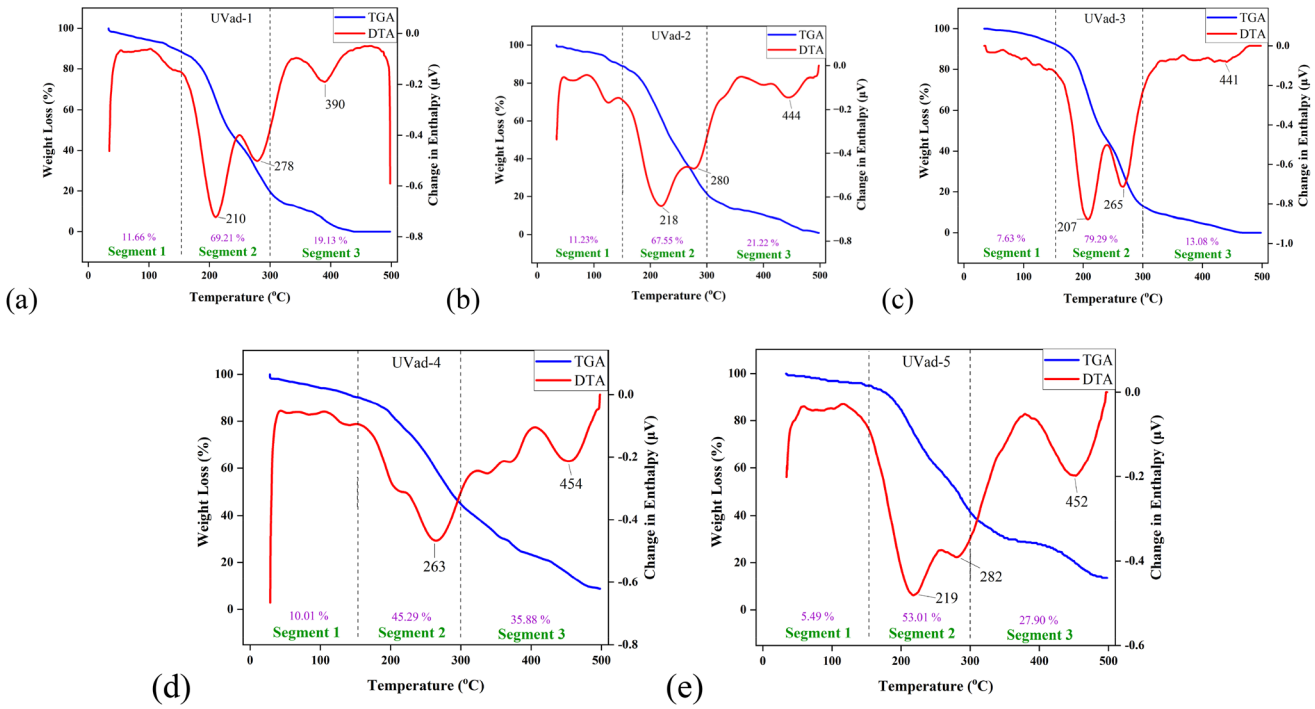

Fig. 3 TGA and DTA combined spectra of UVad-1 (a), UVad-2 (b), UVad-3 (c), UVad-4 (d) and UVad-5 (e).

Reduced weight loss in UVad-3 and UVad-5 suggests improved thermal stability till 150 °C, likely due to less volatile components. This stability might have contributed to their low WAC values.

All samples exhibited significant weight losses in the second segment, indicating a breakdown of the polymeric network in adhesives. Weight losses observed in second segment for UVad-1, UVad-2, UVad-3, UVad-4, and UVad-5 have been 69.21%, 67.55%, 79.29%, 45.29%, and 53.01%, respectively. In second segment, UVad-3 presented the highest weight loss, whereas UVad-4 presented the least, which is likely indicative of differences in cross-linking density and degradation pattern of different hydroxylated plant oils. It might be considered as one of the reasons, which is counter confirmed by their GC.

In third segment, observed weight losses indicated degradation of remaining aromatic network, leaving behind unoxidizable residues. Final weight losses observed for UVad-1, UVad-2, UVad-3, UVad-4, and UVad-5 have been 19.13%, 20.28%, 13.08%, 35.88%, and 27.90%, respectively. In third segment, the least degradation in UVad-3 demonstrates the lowest aromatic content in comparison to other samples. On contrary, the highest degradation rates observed in UVad-4 and UVad-5 suggest high aromatic content that disintegrated at elevated temperatures.

For a better understanding of thermal degradation behavior in all adhesives, DTA spectra are presented in Fig. 3. Data showed three main decomposition processes in thermal degradation profiles of adhesive samples. First decomposition was observed between 200–220 °C, with highest intensity, corresponding to PU depolymerisation.[42] Second decomposition with slightly less intensity was observed at about 260–280 °C, attributed to polyol and isocyanate degradation.[42] Third decomposition with the least intensity was observed between 390–450 °C, indicating breakdown of thermally stable TDI structure with aromatic rings, isocyanate moieties, and methylene bridges.[43] DTA spectra of UVad-1 and UVad-5 presented sharp, well-defined peaks for all three distinct processes, which might be attributed to homogenised sample compositions. Contrarily, the other three samples showed diffused peaks for some of these transitions.

4.2.3 DSC. DSC spectra of all samples (Fig. 4) displayed endothermic peaks, referring to glass transition of hard segment (Tg_H), melting temperature (T_m), and degradation temperature (T_d). The difference in thermal transitions observed in all five samples reflected the difference in molecular compositions and cross-linking densities. First endotherm in DSC spectra of adhesives near 100 °C is attributed to the change of aggregation of hard segment.[44] DSC study of adhesive samples UVad-1 to UVad-4 showed Tg_H at 117.50 °C, 112.80 °C, 116.50 °C, and 120.50 °C, respectively. Data revealed that UVad-5 curve lacked a distinct Tg_H peak, potentially due to the lowest TDI % mole ratio compared to the other formulations. Despite lack of a sharp Tg_H, UVad-5 showed considerable thermal transitions.

UVad-1 to UVad-5 showed a range of T_m from 207 to 219 °C. This variation in T_m among the samples shows different molecular connectivity, which likely influences depolymerisation behavior.[55] Data showed that UVad-4 lacked a well-defined T_m, which might be attributed to the presence of CaO among the ingredients, notorious for high density and step-growth polymerisation reaction,[45] therefore not supportive in building huge polymers. Sample UVad-3 exhibited a sharp and well-

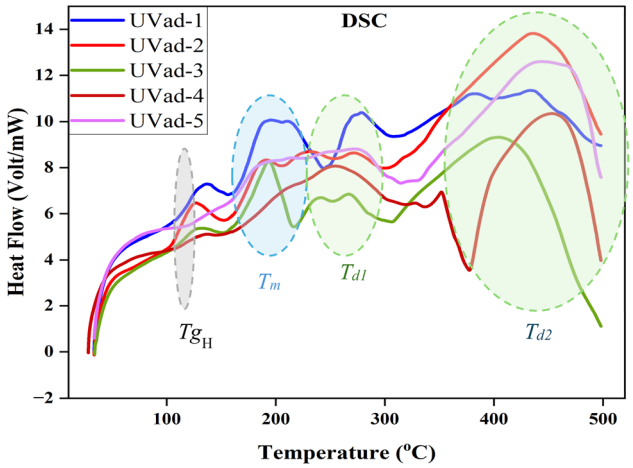

Fig. 4 Comparative DSC analysis of all adhesive samples.

defined T_m, likely due to nearly equal and relatively low polyol density, combined with high hydroxyl contents of HEuO, resulting in a more ordered polymeric network. Samples UVad-1 and UVad-2, which were made of same ingredients but varying mole ratios, exhibited a clear difference in T_m profiles. Specifically, UVad-1, with a higher MSO concentration, exhibited a prominent T_m peak, which is slightly split, whereas UVad-2, with a higher EuO concentration, displayed a diffused T_m peak, which was characterised by two distinct maxima. These differences indicate differences in bond formation, as shown in Scheme 1. Sample UVad-5 had a broad and non-segmental peak for melting and decomposition, likely caused by high viscosity of HMSO, which prevents large polymer chains from forming. Despite this, high functionality facilitated the development of a cross-linked network, which might also be associated with hydrogen bond formation.[56]

Endothermic peaks from 250 °C onwards corresponded to degradation temperatures, which fell into two distinct sets: below 300 °C, attributed to the segregation of polyol and isocyanate groups, and above 300 °C, attributed to degradation of hard segments of aromatic components.[57]

To summarise, UVad-4 and UVad-5 show improved resistance to deterioration at high temperatures because of their increased cross-linking density and thermal stability. On the other hand, UVad-1 and UVad-3 show less thermal resistance and a weaker cross-linking structure due to their lower thermal transitions. Variations in UV-triggered detachment characteristics account for the observed variation among samples. In particular, two thermally stable and cross-linked adhesives, UVad-4 and UVad-5, showed better resistance to heat and UV-induced degradation.

4.2.4 WAC and GC. WAC and GC data (Table 4) of prepared adhesives showed a significant difference, indicating compositional and inter-connectivity differences. Despite absorbing 10.71% water at 48 h, initial decrease in WAC and low GC of UVad-1 suggested the existence of uncured components, compromising its stability when exposed to moisture over a prolonged period of time; UVad-2 showed a similar but slightly better WAC pattern, with a peak absorbance value of 15.51% after 48 h, accompanied by a slightly better GC. A decreased MSO concentration in UVad-2 may explain this increase in comparison to UVad-1. UVad-3 had the lowest WAC with a peak value of 3.93% at 48 h, though it had slightly better GC. This might be attributed to the hydrophobic nature of both MSO and HEuO (while the high functionality and density of the network likely hindered DCM penetration). UVad-4 showed a similar behaviour, with a WAC peak of 5.73% at 3 h and then a decrease, indicating first water absorption due to high-density CaO, which in turn degraded or melted. This high density may also have led to the sample's highest GC. UVad-5 showed a clear WAC pattern, manifested by an initial increase, followed by a decrease, and finally another increase reaching a maximum absorption of 7.46% after 72 h. This pattern implies that the sample was initially free of uncured material so that it absorbs water. The subsequent reduction in WAC was a sign of structural disintegration, which stopped once a particular component degraded, allowing further water absorption. Higher GC value implies a dense molecular structure with a good level of cross-linking, which usually decreases solubility and increases stability in DCM.

4.2.5 Morphology. Morphological analysis of prepared samples was performed at macrophasic and microparticulate levels using microscopy and scanning electron microscopy (SEM), respectively (Fig. 5). Microscopic examination provided insight into the mixing quality of ingredients, while SEM imaging provided a deeper understanding of the molecular organisation of components. Microscopic analysis showed significant variation in surface textures, reflecting differences in ingredient homogeneity and formulation. Specifically, different surface morphologies were observed: UVad-1 had a slightly

Table 4 WAC (%) and GC (%) of adhesive samples

	WAC (%)							
Sample ID	1 h	2 h	3 h	4 h	24 h	48 h	72 h	GC (%)
UVad-1	−2.77[a]	−7.54[a]	−8.73[a]	−10.32[a]	7.14	10.71	−4.36[a]	78.92
UVad-2	−1.38[a]	−2.06[a]	−3.10[a]	−4.13[a]	10.00	15.51	8.62	84.78
UVad-3	0.91	2.71	2.11	−1.51[a]	2.71	3.93	−9.48[a]	81.01
UVad-4	3.27	4.92	5.73	4.92	3.28	1.64	−7.38[a]	89.03
UVad-5	2.99	5.97	2.99	1.49	−1.49[a]	4.48	7.46	85.10

[a] Dissolution of the samples was observed at some stages.

wrinkled surface (Fig. 5a); UVad-2 had a smooth surface (Fig. 5c); while UVad-3 (Fig. 5e), UVad-4 (Fig. 5g), and UVad-5 (Fig. 5i) had surfaces with holes, cracks, and flakes, respectively. Surface uniformity and smoothness indicate a well-blended macrophasic composition, whereas damaged surfaces suggest macrophasic heterogeneous separation of ingredients in sample.

SEM analysis of five samples revealed two general morphologies: needle-shaped structures and lump-like domains. The lump-like appearance may be related to increased crosslinking density, localised phase separation, or brittle fracture, whereas the needle-like features may result from oriented polymer domains or irregular curing. Correlating SEM analysis with UV-responsive detachment, it has been noticed that samples with needle-shaped structures presented UV-responsive detachment, demonstrating the crucial role of internal crosslinking in adhesive performance. UVad-1 (Fig. 5b) and UVad-3 (Fig. 5f) showed a morphology consisting of a lump-like structure. These samples showed no UV-responsive detachment, probably because of an agglomerated structure that has no requisite functional groups for such detachments. SEM analysis of UVad-2 (Fig. 5d), UVad-4 (Fig. 5h), and UVad-5 (Fig. 5j) showed that they had needle-shaped structures, indicating that they have significant crosslinking, which is related to their ability to withstand multiple bonding–debonding cycles.

4.2.6 Mechanical testing. Mechanical evaluation of UV-responsive adhesives (UVad-1 to UVad-5) was performed to determine their load-bearing capacity and resistance to pressure. Normalisation of force was carried out in order to achieve a comparative analysis of load-bearing capacity between several cycles of de-adhesion and reattachment.[6] A small quantity of each sample (0.08 g) was utilised to bond two slides, and subsequently, their capacity to withstand a load before SLJ failure was assessed by applying different load levels.

UVad-1 showed a load-bearing capacity of up to 3.95 kg with a normalised force of 1 in fourth cycle. UVad-2 demonstrated an enhanced load-bearing capacity as compared to UVad-1 and reached a maximum loading of 4.45 kg with a normalised power of 1 in fifth cycle. A gradual rise in pressure and normalised force through cycles is suggestive of improvement in reattachment and bonding consistency. This improved performance could be attributed to a change in composition. However, the performance of UVad-3 was reduced compared to UVad-2 and attained a maximum load of 3.9 kg, with a normalised force of 1 for first cycle. Load-bearing capacity and mechanical strength were decreased gradually thereafter. UVad-4 showed a certain moderate level of performance, with a maximum load of 2.5 kg, having a normalised force of 1 during fourth cycle. Addition of HSSO in this sample has resulted in improved UV responsiveness but decreased its mechanical performance in comparison to its previous samples. Lastly, UVad-5 exhibited a load-bearing capacity of 3.85 kg with a normalised force of 1 in sixth cycle. Mechanical strength was slowly increased, showing an enhancement in mechanical performance. Impressive performance highlighting the efficacy of HMSO and EuO for improving mechanical strength and UV responsiveness. Mechanical

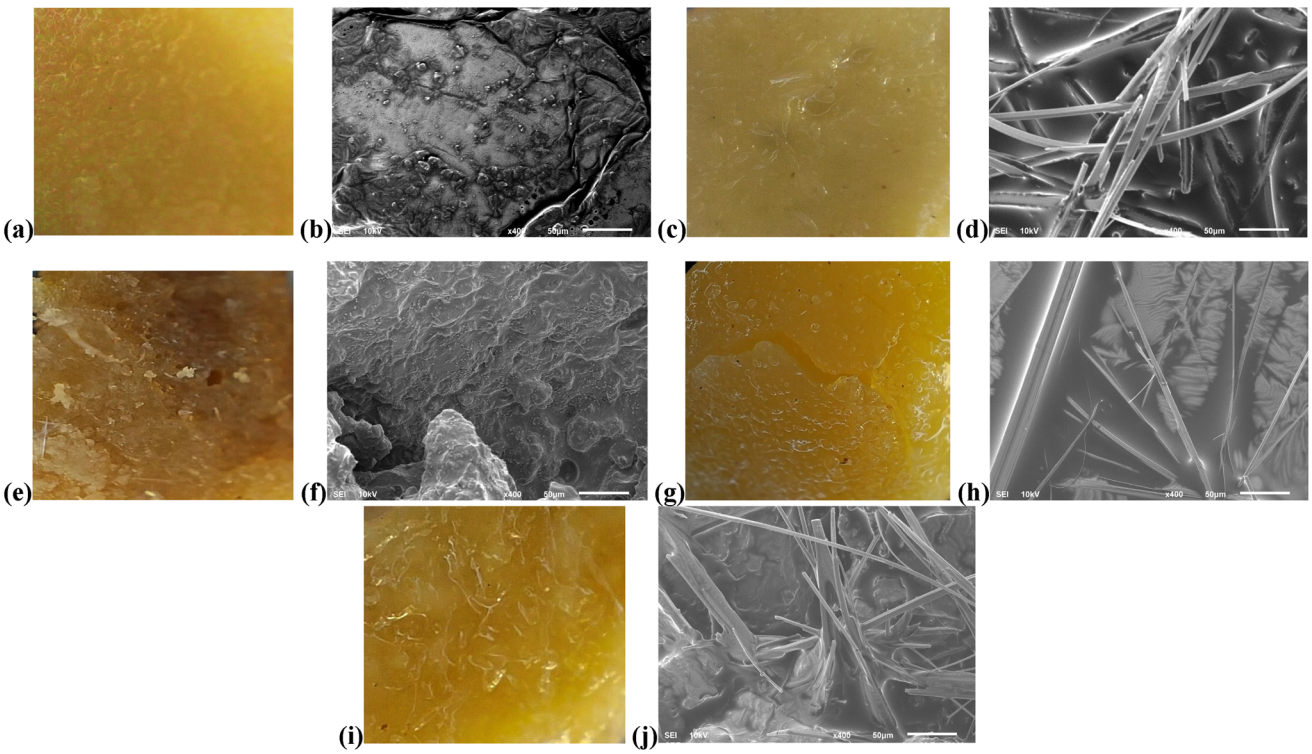

Fig. 5 Microscopic and SEM images of UVad-1 (a and b), UVad-2 (c and d), UVad-3 (e and f), UVad-4 (g and h), UVad-5 (i and j).

evaluation highlights continuous enhancement of adhesive properties from UVad-1 to UVad-5, with UVad-5 standing out as the most effective sample. Findings indicated that modified oils have a considerable effect on adhesive strength, durability, and reusability, suitable for applications that require frequent detachment and reattachment (Table 6).

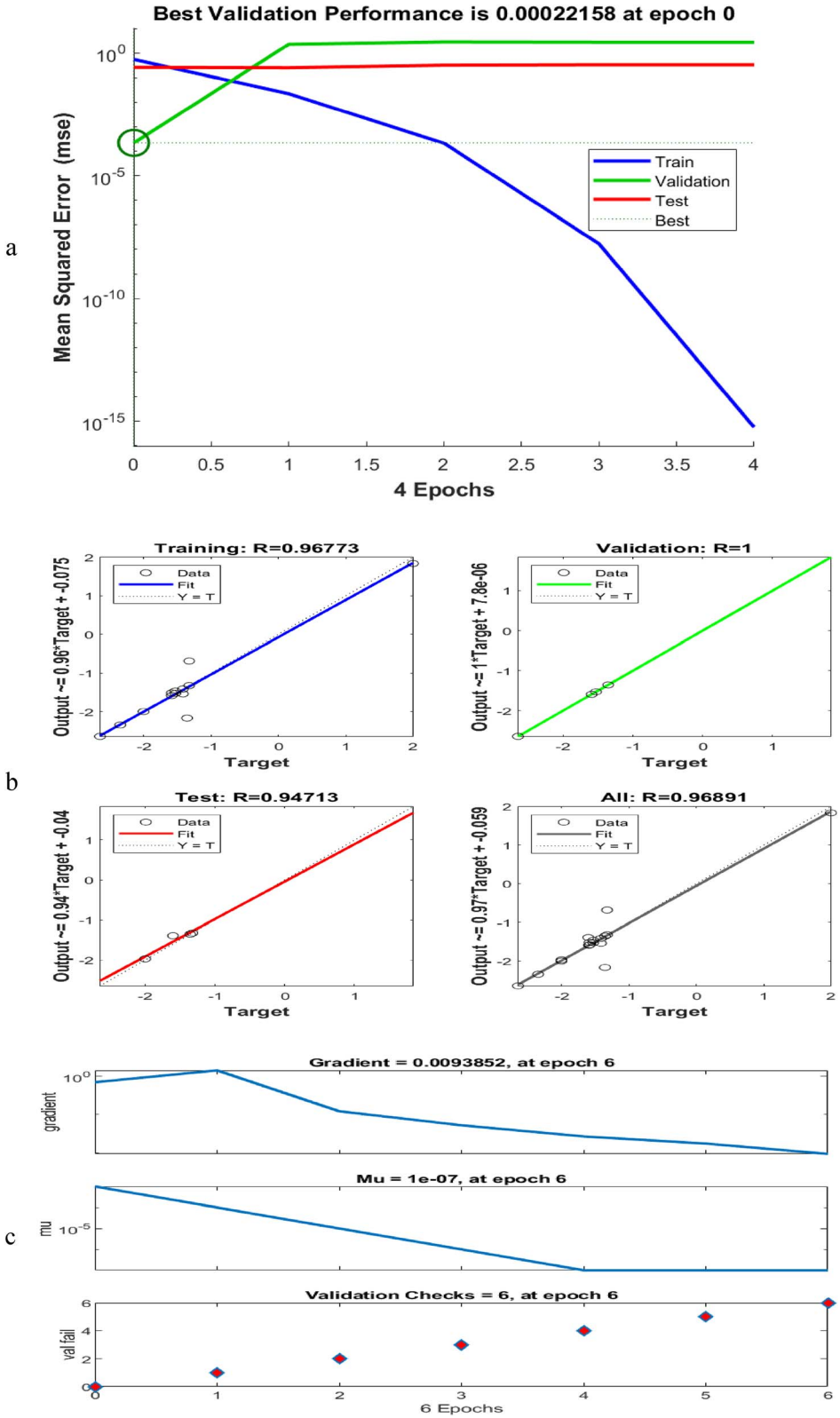

Fig. 6 (a) Performance graph, (b) regression analysis, (c) ANN trained data for mechanical test.

Table 5 Mechanical strength evaluation of prepared samples

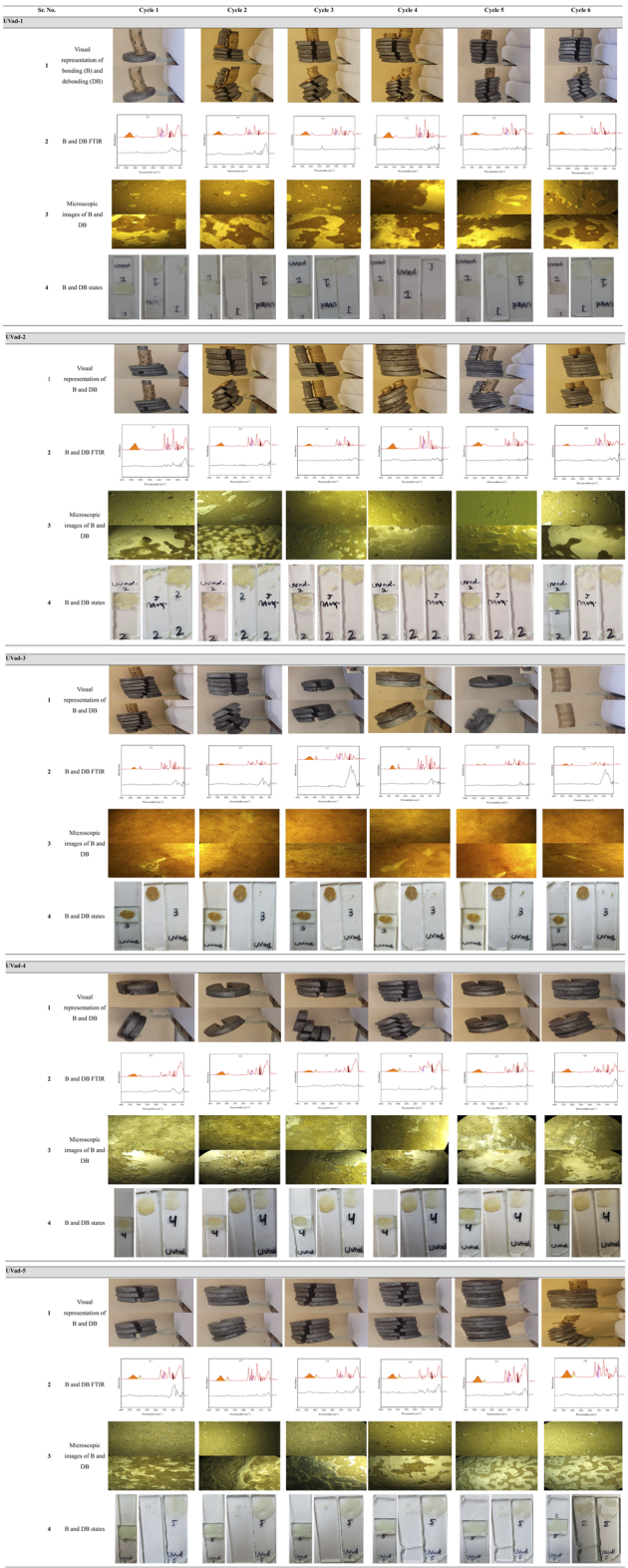

Mechanical testing evaluation was conducted to determine the bonding strength of prepared adhesives, and their maximum weight-bearing capacity for multiple cycles is given in Table 5.

4.2.7 Statistical analysis. For each adhesive sample, mean, SD, and CV have been calculated (Table 7) to evaluate cycle-to-cycle variability in mechanical performance. Mean applied

Table 6 : Mechanical load-bearing analysis of prepared adhesives

	No. of cycles	Sample weight (g)	Length (mm)	Width (mm)	Area (mm^2)	Area (m^2)	Thickness (mm)	Load (kg)	Applied stress σ (KN m^{-2})	Normalised force (F_N)
UVad-1	C1	0.08	20.55	23.12	475.12	0.0004751	0.13	0.95	19595.21	0.00
	C2		20.55	23.14	475.53	0.0004755	0.12	2.95	60795.71	0.67
	C3		20.56	23.14	475.76	0.0004758	0.11	2.8	57676.33	0.62
	C4		20.56	23.17	476.38	0.0004764	0.10	3.95	81259.48	1.00
	C5		20.57	23.20	477.22	0.0004772	0.08	3.8	78034.63	0.95
	C6		20.60	23.20	477.92	0.0004779	0.07	3.8	77920.99	0.95
UVad-2	C1	0.08	19.20	21.55	413.76	0.0004138	0.17	2.75	65134.38	0.11
	C2		19.26	21.56	415.25	0.0004152	0.16	2.55	60181.25	0.00
	C3		19.27	21.58	415.85	0.0004158	0.14	3.45	81304.02	0.47
	C4		19.27	21.58	415.85	0.0004158	0.13	3.7	87195.61	0.61
	C5		19.28	21.59	416.26	0.0004163	0.13	4.45	104767.46	1.00
	C6		19.30	22.00	424.6	0.0004246	0.11	4	92322.19	0.72
UVad-3	C1	0.08	15.1	16.55	249.905	0.0002499	0.22	3.9	152938.12	1.00
	C2		15.13	16.56	250.553	0.0002506	0.21	2.5	97783.78	0.60
	C3		15.2	16.59	252.168	0.0002522	0.19	1	38862.98	0.17
	C4		15.22	16.62	252.956	0.000253	0.18	1	38741.85	0.17
	C5		15.25	16.63	253.608	0.0002536	0.17	0.5	19321.20	0.03
	C6		15.26	16.65	254.079	0.0002541	0.15	0.4	15428.27	0.00
UVad-4	C1	0.08	18.62	17.90	333.298	0.0003333	0.14	1	29403.12	0.25
	C2		18.65	17.91	334.022	0.000334	0.13	0.5	14669.71	0.00
	C3		18.68	17.93	334.932	0.0003349	0.12	1.5	43889.45	0.50
	C4		18.71	17.95	335.845	0.0003358	0.10	2.5	72950.43	1.00
	C5		18.73	17.96	336.391	0.0003364	0.09	1	29132.78	0.25
	C6		18.75	17.99	337.313	0.0003373	0.08	2	58106.36	0.75
UVad-5	C1	0.08	21.96	25.85	567.666	0.0005677	0.21	1.5	25895.51	0.00
	C2		21.96	25.86	567.886	0.0005679	0.21	2	34513.99	0.21
	C3		21.92	25.88	567.29	0.0005673	0.20	2.5	43187.82	0.43
	C4		21.93	25.90	567.987	0.000568	0.19	3	51761.75	0.64
	C5		21.96	25.91	568.984	0.000569	0.17	3.5	60282.93	0.85
	C6		21.99	25.93	570.201	0.0005702	0.15	3.85	66169.68	1.00

stress values ranged from 38 692 KN m^{-2} (UVad-4) to 79 212 KN m^{-2} (UVad-2). SD reflected the dispersion of individual cycle data around respective means, while CV enabled direct comparison of relative variability among samples. Among the five formulations, UVad-2 exhibited the most consistent performance (CV = 20.6%), whereas UVad-3 showed the highest variability (CV = 87.7%). Subsequently, an artificial neural network (ANN) model was developed using statistical parameters as inputs to predict target stress. At epoch 0, the ANN's best validation mean squared error (MSE) was 0.00022158. Its correlation coefficients for training, validation, testing, and combined dataset were 0.96773, 1.000, 0.94713, and 0.96891, respectively. These findings suggest that the combination of statistical analysis and ANN modelling offers a reliable way for assessing the mechanical reliability of adhesives subjected to cyclic loading conditions (Fig. 6).

Table 7 Statistical analysis parameters for mechanical strength evaluation

	Input data			Output data		
Sample	Mean	SD	CV	Target stress	ANN	Error
UVad-1	72 713	22 981	31.6	72 713	−1.4379	0.067479
UVad-2	79 212	16 311	20.6	79 212	−1.432	−0.015072
UVad-3	57 162	50 147	87.7	57 162	−1.3918	−0.004376
UVad-4	38 692	22 636	58.5	38 692	−1.4437	0.09262
UVad-5	44 569	14 788	33.2	44 569	−1.4986	−0.0068324

4.3 UV detachment analysis

All prepared samples have been analysed for UV-responsive detachment and thermal reattachment cycles. A specific amount of samples (0.05 g each) has been utilised for glass slide attachments in form of SLJ. Each sample's slide was then subjected to UV irradiation until detachment (Table 8). UV irradiation was carried out using a setup equipped with a 365 nm UV lamp (20 mW cm^{-2}), where bonded samples were placed at a distance of approximately 4–5 cm inside a wooden enclosure. Samples UVad-1 and UVad-3 exhibited no detachment when exposed to UV irradiation. However, other three samples exhibited UV-responsive detachment. UVad-2 demonstrated 4 maximum cycles, UVad-4 exhibited 10 cycles with gradually increasing detachment time, and UVad-5 also showed continued detachment for 12 cycles with increasing detachment

Table 8 UV-responsive detachment analysis of prepared samples

Sample ID	Cycle	Pictorial representation with UV irradiation time								
UVad-1	C1	No DB								
UVad-2	C1	0 sec	1 min	2 min	3 min	3 min 30 sec	3 min 45 sec	3 min 46 sec	3 min 47 sec	
	C2	0 sec	1 min	2 min	3 min	4 min	5 min	5 min 28 sec	5 min 29 sec	
	C3	0 sec	1 min	2 min	3 min	4 min	5 min	6 min 1 sec	6 min 2 sec	6 min 3 sec
	C4	0 sec	1 min	2 min	3 min	4 min	5 min	6 min	7 min	8 min
		8 min 10 sec	8 min 11 sec	8 min 12 sec	8 min 13 sec					
UVad-3	C1	No DB								
UVad-4	C1	0 sec	10 sec	19 sec	20 sec	21 sec	21.5 sec	23 sec		
	C2	0 sec	10 sec	20 sec	21 sec	22 sec	24 sec			
	C3	0 sec	10 sec	20 sec	30 sec	35 sec	36 sec	37 sec	39 sec	
	C4	0 sec	10 sec	20 sec	30 sec	35 sec	36 sec	37 sec	39 sec	
	C5	0 sec	10 sec	20 sec	40 sec	42 sec	43 sec	44 sec	46 sec	
	C6	0 sec	10 sec	20 sec	50 sec	58 sec	59 sec	1 min	1 min 1 sec	1 min 2 sec
	C7	0 sec	10 sec	20 sec	40 sec	58 sec	1 min	1 min 1 sec	1 min 3 sec	
	C8	0 sec	10 sec	20 sec	1 min	1 min 15 sec	1 min 20 sec	1 min 21 sec	1 min 22 sec	1 min 23 sec
	C9	0 sec	10 sec	20 sec	1 min	1 min 20 sec	1 min 21 sec	1 min 22 sec	1 min 23 sec	1 min 24 sec
	C10	0 sec	10 sec	20 sec	1 min	1 min 30 sec	1 min 31 sec	1 min 32 sec	1 min 33 sec	
UVad-5	C1	0 sec	10 sec	20 sec	40 sec	41 sec	42 sec	43 sec		
	C2	0 sec	10 sec	20 sec	40 sec	1 min 6 sec	1 min 7 sec	1 min 8 sec		
	C3	0 sec	10 sec	20 sec	40 sec	1 min	1 min 10 sec	1 min 11 sec	1 min 12 sec	
	C4	0 sec	10 sec	20 sec	40 sec	1 min	1 min 15 sec	1 min 19 sec	1 min 20 sec	1 min 21 sec
	C5	0 sec	10 sec	20 sec	40 sec	1 min	1 min 20 sec	1 min 21 sec	1 min 22 sec	1 min 23 sec
	C6	0 sec	10 sec	20 sec	40 sec	1 min	1 min 30 sec	1 min 40 sec	1 min 41 sec	1 min 42 sec
	C7	0 sec	30 sec	1 min	1 min 30 sec	2 min	2 min 11 sec	2 min 12 sec	2 min 13 sec	2 min 14 sec
	C8	0 sec	30 sec	1 min	1 min 30 sec	2 min	2 min 20 sec	2 min 21 sec	2 min 22 sec	2 min 23 sec
	C9	0 sec	1 min	2 min	2 min 30 sec	3 min	3 min 30 sec	3 min 31 sec	3 min 32 sec	3 min 33 sec
	C10	0 sec	1 min	2 min	3 min	4 min	4 min 10 sec	4 min 11 sec	4 min 12 sec	4 min 13 sec
	C11	0 sec	1 min	2 min	3 min	4 min	5 min	5 min 2 sec	5 min 3 sec	5 min 4 sec
	C12	0 sec	1 min	2 min	4 min	6 min	6 min 55 sec	6 min 56 sec	6 min 57 sec	6 min 58 sec

time. When examining the time of detachment in relation to UV irradiation, all samples demonstrated a rise in time corresponding to an increasing number of cycles. UVad-2 detached at 3 min and 47 s during first cycle under 571.07 KN m^{-2} force and at 8 min and 13 s during fourth cycle under 560.33 KN m^{-2} force. Sample UVad-4 exhibited the fastest detachment, taking

Table 9 Visual representation, FTIR, and microscopic analysis for the respective cycles in UV detachment of samples

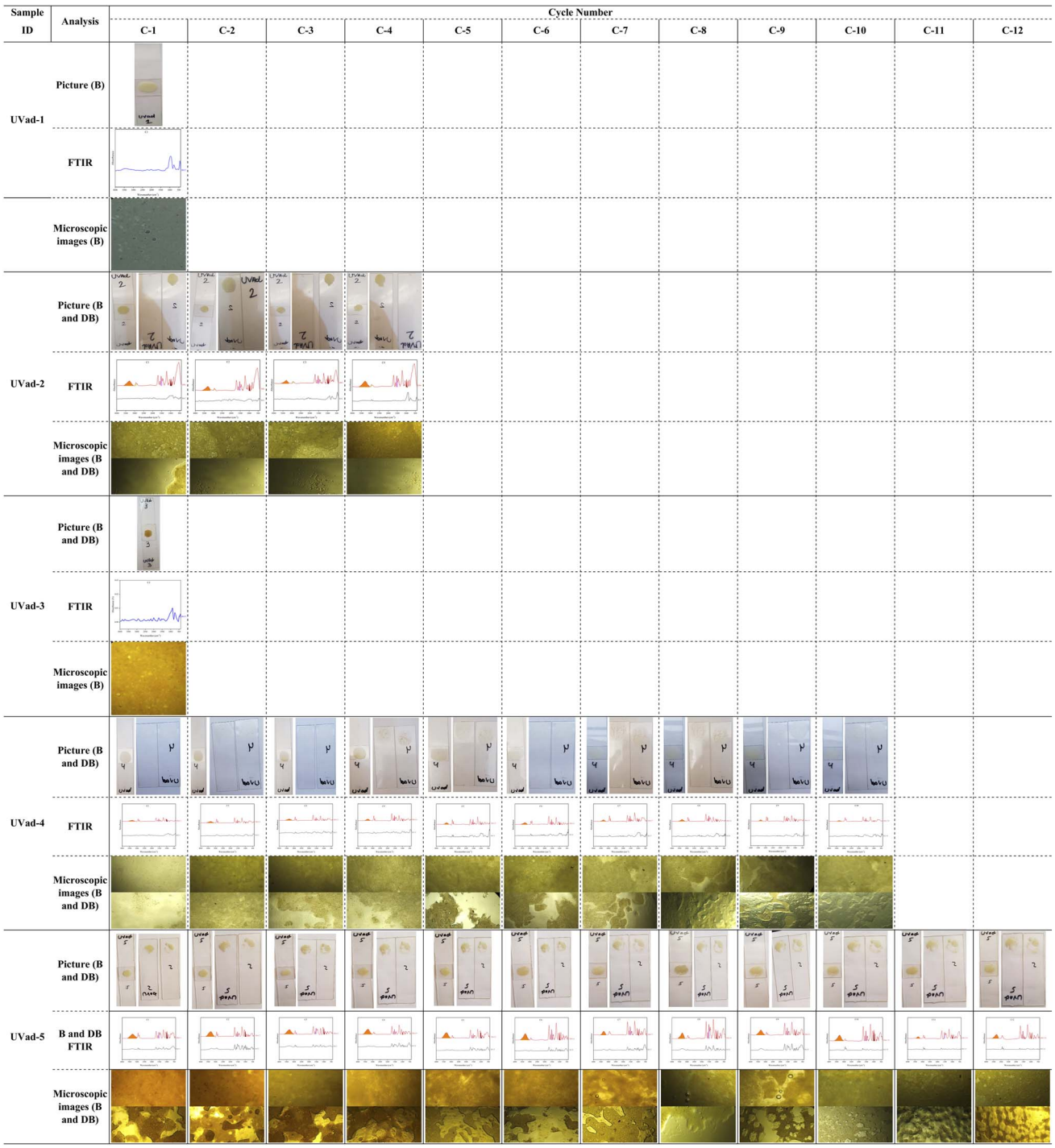

23 s for first cycle under 675.23 KN m^{-2} force and 1 min and 33 s for the tenth cycle under 638.79 KN m^{-2} force. Sample UVad-5 demonstrated detachment ranging from 43 s in first cycle under 562.44 KN m^{-2} force to 6 min and 58 s in twelfth cycle under 532.97 KN m^{-2} force. Compositional differences between these two samples, which utilise different plant oils, expose a significant improvement in their chemistry and UV-responsiveness concerning detachable adhesives. Notable thing is the fact that, all prepared adhesive formulations had a repeated detachability under mechanical load conditions.

All samples were analysed in FTIR in bonding and debonding states while undergoing UV-responsive cycles of detachment. This test was done to study the chemical differences between bonded and debonded states. Data presented in Table 9 indicate that after debonding, all samples exhibited three distinct peaks at 1048 cm^{-1} (C–O),[4] 1533 cm^{-1} (alkene),[41] and

Table 10 Physical parameters of adhesives for UV-responsive debonding

Sample ID	Cycles	Sample weight (g)	Length (mm)	Width (mm)	Area (mm^2)	Thickness (mm)	Load (kg)	Applied stress σ (kN m^{-2})	Detachment time
Uvad-1	C1	0.05	11.53	11.92	137.44	0.26	0.01	713.05	No DB
Uvad-2	C1	0.05	13.05	13.15	171.61	0.17	0.01	571.07	3 min 47 s
	C2		13.11	13.19	172.92	0.15		566.73	5 min 29 s
	C3		13.14	13.25	174.11	0.14		562.88	6 min 3 s
	C4		13.17	13.28	174.90	0.12		560.33	8 min 13 s
Uvad-3	C1	0.05	13.51	12.87	173.87	0.19	0.01	563.63	No DB
Uvad-4	C1	0.05	11.41	12.72	145.14	0.25	0.01	675.23	23 s
	C2		11.43	12.75	145.73	0.24		672.46	24 s
	C3		11.46	12.79	146.57	0.21		668.61	39 s
	C4		11.50	12.83	147.55	0.19		664.20	39 s
	C5		11.51	12.85	147.91	0.18		662.59	46 s
	C6		11.53	12.88	148.51	0.17		659.90	1 min 2 s
	C7		11.57	12.92	149.48	0.16		655.59	1 min 3 s
	C8		11.60	12.95	150.22	0.15		652.38	1 min 23 s
	C9		11.65	12.99	151.33	0.13		647.58	1 min 24 s
	C10		11.72	13.09	153.41	0.10		638.79	1 min 33 s
Uvad-5	C1	0.05	13.20	12.22	161.30	0.23	0.01	562.44	43 s
	C2		13.22	12.25	161.95	0.21		560.74	1 min 8 s
	C3		13.23	12.27	162.33	0.20		559.89	1 min 12 s
	C4		13.26	12.30	163.10	0.19		557.36	1 min 21 s
	C5		13.28	12.32	163.49	0.19		555.69	1 min 23 s
	C6		13.28	12.33	163.74	0.18		555.69	1 min 42 s
	C7		13.30	12.36	164.39	0.16		554.02	2 min 14 s
	C8		13.31	12.37	164.64	0.15		553.18	2 min 23 s
	C9		13.34	12.40	165.42	0.13		550.70	3 min 33 s
	C10		13.40	12.48	167.36	0.11		545.78	4 min 13 s
	C11		13.50	12.55	169.43	0.10		537.72	5 min 4 s
	C12		13.56	12.61	170.99	0.09		532.97	6 min 58 s

3200 cm^{-1} (OH).[42] This indicated that UV-based separation of adhesives is at a location where alkene and hydroxyl components are produced. Physical parameters of adhesives, tested during UV-responsive debonding, are presented in Table 10.

5 Conclusion

This research successfully synthesised UV-responsive, bio-based adhesives derived from plant oils to create temporary binding while increasing environmental sustainability. Of the five samples, UVad-4 and UVad-5 showed exceptional reusability, latter being found to maintain numerous cycles of detachment (due to UV) and reattachment (due to thermal treatment). Formulation of UVad-5, which includes HMSO and EuO, has been optimised to improve adhesive strength and detachability, making it suitable for frequent separation. EuO and HMSO functioned as natural plasticisers for flexibility and durability against UV radiation. This study points out the potential of bio-based adhesives for temporary but strong bonding applications. This provides opportunities for further research on plant oil derivatives in the domain of advanced and sustainable adhesive technologies.

Conflicts of interest

There are no conflicts to declare.

Data availability

Data will be made available on request.

References

1 M. Sługocka, *et al.*, Study of the Impact of Surface Topography on Selected Mechanical Properties of Adhesive Joints, *Coatings*, 2024, **14**(8), 944.
2 N. Karthikeyan and J. Naveen, Effect of surface modified adherend and nanofiller modified adhesives on the shear behaviour of single lap joints: a mini review, *J. Adhes. Sci. Technol.*, 2024, **38**(21), 3943–3962.
3 F. Gubbels, An overview of the chemistry of condensation curing silicone sealants and adhesives, *Int. J. Adhes. Adhes.*, 2024, **132**, 103728.
4 M. Atif, *et al.*, Synthesis and characterisation of sesame oil based plasticisers for reversible bonding in thermally detachable polyurethane adhesives, *Sustain. Mater. Technol.*, 2024, **39**, e00793.

5 Y. L. Tan, *et al.*, Adhesion Evolution: Designing Smart Polymeric Adhesive Systems with On-Demand Reversible Switchability, *ACS Nano*, 2024, **18**(36), 24682–24704.
6 M. Atif, *et al.*, Thermally stimulated bio-acrylate based detachable adhesives with sustainable bonding-debonding design, *Int. J. Adhes. Adhes.*, 2025, **136**, 103853.
7 Q. Yan, M. Zhou and H. Fu, A reversible and highly conductive adhesive: towards self-healing and recyclable flexible electronics, *J. Mater. Chem. C*, 2020, **8**(23), 7772–7785.
8 I. Bibi, *et al.*, A comprehensive study of electrically switchable adhesives: Bonding and debonding on demand, *Mater. Today Commun.*, 2023, **35**, 106293.
9 J. G. Kim, *et al.*, A novel wafer level bonding/debonding technique using an anti-adhesion layer for polymer-based zero-level packaging of RF device, in *2010 Proceedings 60th Electronic Components and Technology Conference (ECTC)*, 2010.
10 Y. Xue, *et al.*, Trigger-Detachable Hydrogel Adhesives for Bioelectronic Interfaces, *Adv. Funct. Mater.*, 2021, **31**(47), 2106446.
11 M. Abbasi, R. Ciardiello and L. Goglio, Backface strain as an index to detect damage initiation in composite single-lap bonded joints: Effects of adhesive type and joint dimensions, *Int. J. Adhes. Adhes.*, 2024, **134**, 103791.
12 M. Muqaddas, *et al.*, Advances in Debondable Adhesives: A Focus on pH-Dependent Reversible Bonding Technologies, *Polym. Rev.*, 2025, 1–46.
13 D. Kim, *et al.*, Ultraviolet Light Debondable Optically Clear Adhesives for Flexible Displays through Efficient Visible-Light Curing, *Adv. Mater.*, 2024, **36**(14), 2309891.
14 G. Wang, *et al.*, Enabling (De)bonding on-demand with optically switchable pressure sensitive adhesive tape *via* photodimerisation, *Chem. Eng. J.*, 2024, **499**, 155820.
15 A. M. S. Couto, *et al.*, Exploring Bio-Based Polyurethane Adhesives for Eco-Friendly Structural Applications: An Experimental and Numerical Study, *Polymers*, 2024, **16**(17), 2546.
16 B. Ali, A. Irshad and M. Atif, Bio-based photo-curable polyurethane composites, *Polym. Adv. Technol.*, 2023, **34**(2), 452–473.
17 H. Zhu, *et al.*, Robust, reusable, and antioxidative supramolecular adhesive to inorganic surfaces based on water-stimulated hydrogen bonding, *ACS Appl. Polym. Mater.*, 2022, **4**(3), 1586–1594.
18 K. A. Bovaldinova, *et al.*, Thermo-switchable pressure-sensitive adhesives with strong tunable adhesion towards substrate surfaces of different hydrophilicity, *Polymer*, 2017, **125**, 10–20.
19 J. Min and J. Qu, Optically clear pressure-sensitive adhesive with flexible crosslinking agent for high recovery efficiency, low energy storage modulus, and excellent folding resistance, *Polym. Adv. Technol.*, 2024, **35**(9), e6574.
20 L. Alfhaid, *et al.*, Double-network hydrogels improve pH-switchable adhesion, *Soft Matter*, 2016, **12**(22), 5022–5028.
21 A. Badía, *et al.*, Easy removable and UV tunable biobased waterborne pressure sensitive adhesives, *Int. J. Adhes. Adhes.*, 2021, **108**, 102860.
22 H. Rong, *et al.*, On-demand detachable and reuseable adhesives assembled by organic-silicon nanogels with wide applicability and excellent harsh-environment resistance, *Chem. Eng. J.*, 2024, **498**, 155566.
23 S. Salimi, *et al.*, Composite polyurethane adhesives that debond-on-demand by hysteresis heating in an oscillating magnetic field, *Eur. Polym. J.*, 2019, **121**, 109264.
24 R. Belouadah, *et al.*, Phase switching phenomenon in magnetoelectric laminate polymer composites: Experiments and modeling, *Phys. B*, 2011, **406**(14), 2821–2826.
25 M. D. Banea, L. F. M. da Silva and R. J. C. Carbas, Debonding on command of adhesive joints for the automotive industry, *Int. J. Adhes. Adhes.*, 2015, **59**, 14–20.
26 E. Gkartzou, *et al.*, Induction Heating of Laminated Composite Structures with Magnetically Responsive Nanocomposite Interlayers for Debonding-on-Demand Applications, *Polymers*, 2024, **16**(19), 2760.
27 Y. Wei, *et al.*, Electrically Detachable Ionic Conductive Epoxy Adhesives with High Bonding Strength, *ACS Appl. Polym. Mater.*, 2023, **5**(9), 7328–7339.
28 S. Sun, *et al.*, Charge Delocalization for Electrically Detachable Poly(ionic liquids) Ionoadhesives with Ultrahigh Mechanical Robustness, *Macromolecules*, 2024, **57**(19), 9355–9366.
29 Q. Zhu, *et al.*, In-process ultrasonic inspection of first layer detachment during additive manufacturing, *Int. J. Adv. Des. Manuf. Technol.*, 2022, **121**(11), 8341–8356.
30 Z. Zhou and C. Chen, Research advances in the ultrasonic–assisting adhesive bonding, *J. Manuf. Process.*, 2024, **110**, 134–160.
31 W. Xiangjun, *et al.*, A thermoreversible crosslinking hot-melt adhesive: reversibility and performance, *RSC Adv.*, 2021, **11**(52), 32565–32572.
32 L. M. Sridhar, *et al.*, Re-usable thermally reversible crosslinked adhesives from robust polyester and poly(ester urethane) Diels–Alder networks, *Green Chem.*, 2020, **22**(24), 8669–8679.
33 G. Xu, *et al.*, Photoswitchable Adhesives Using Azobenzene-Containing Materials, *Chem. - Asian J.*, 2020, **15**(5), 547–554.
34 J. Wang, *et al.*, Preparation of UV Debonding Acrylate Adhesives by a Postgrafting Reaction, *Materials*, 2023, **16**(17), 5911.
35 J. T. Lai, D. Filla and R. Shea, Functional polymers from novel carboxyl-terminated trithiocarbonates as highly efficient RAFT agents, *Macromolecules*, 2002, **35**(18), 6754–6756.
36 N. D. Blelloch, H. J. Yarbrough and K. A. Mirica, Stimuli-responsive temporary adhesives: enabling debonding on demand through strategic molecular design, *Chem. Sci.*, 2021, **12**(46), 15183–15205.
37 Z. Liu, *et al.*, Efficient utilisation of peach gum to prepare UV-responsive peelable pressure-sensitive adhesives for

non-destructive fabrication of ultrathin electronics, *Appl. Surf. Sci.*, 2023, **612**, 155748.
38 S. V. Pradeep, B. Kandasubramanian and S. Sidharth, A review on recent trends in bio-based pressure sensitive adhesives, *J. Adhes.*, 2023, **99**(14), 2145–2166.
39 Y.-F. Lei, *et al.*, Fully Bio-Based Pressure-Sensitive Adhesives with High Adhesivity Derived from Epoxidised Soybean Oil and Rosin Acid, *ACS Sustain. Chem. Eng.*, 2020, **8**(35), 13261–13270.
40 M. Kim and H. Chung, Photo-responsive bio-inspired adhesives: facile control of adhesion strength *via* a photocleavable crosslinker, *Polym. Chem.*, 2017, **8**(40), 6300–6308.
41 B. Ali, *et al.*, Catalyst-free synthesis of low-temperature thermally actuated shape memory polyurethanes with modified biobased plasticisers, *RSC Adv.*, 2023, **13**(1), 506–515.
42 M. Atif, *et al.*, Cationic UV-Curing of Shape Memory Biobased Polyurethanes Sensing Low Heat, *Polym. Adv. Technol.*, 2024, **35**(10), e6615.
43 F. Febrianto, A. Setianingsih and A. Riyani, Determination of free fatty acid in frying oils of various foodstuffs, *Indones. J. Chem. Environ.*, 2019, **2**(1), 1–6.
44 E. C. Ezeh, *et al.*, Novel Facile Technique for the Determination of Binding Strength of Adhesives, *J. Test. Eval.*, 2019, **47**(5), 3671–3675.
45 B. Jordanov, D. Tsankov and E. H. Korte, Peculiarities in the stretching vibrations of the methylene groups, *J. Mol. Struct.*, 2003, **651–653**, 101–107.
46 N. T. Thanh, Study on effects of isocyanate on some properties of epoxy varnish, *Vietnam J. Chem.*, 2022, **60**(1), 15–20.
47 A. Z. Noor, *et al.*, Synthesis of reusable cement materials through photochemical modification of marble powder for composite structures, *Heliyon*, 2025, **11**(1), e41570.
48 M. Cabo, M. N. Prabhakar and J. I. Song, Synthesis of non-phosphorylated epoxidised corn oil as a novel green flame retardant thermoset resin, *Sci. Rep.*, 2021, **11**(1), 24140.
49 A. Didonna, *et al.*, Infrared Microspectroscopy: A Multiple-Screening Platform for Investigating Single-Cell Biochemical Perturbations upon Prion Infection, *ACS Chem. Neurosci.*, 2011, **2**(3), 160–174.
50 R. Hanumantharaya, I. Sogalad and S. Basavarajappa, Investigations on the influence of nano reinforcement on strength of adhesively bonded joints, *Mater. Today: Proc.*, 2021, **45**, 87–93.
51 K. Kendall, Energizing ASTM lap joint fracture standards, *Philos. Trans. R. Soc., A*, 2021, **379**(2203), 20200287.
52 H. Firmansyah, I. W. Brillian and D. A. Bangga, Adhesive Bonding Analysis of Single Lap Joint Composite E-Glass Fiber WR 600, *IOP Conf. Ser. Earth Environ. Sci.*, 2021, **700**, 012005.
53 E. L. Hanry, *et al.*, Characterisation of biofilms developed from alginate extracted from Padina sp. incorporated with calcium chloride (CaCl2), *J. Phys.: Conf. Ser.*, 2022, **2314**(1), 012022.
54 V. M. Serrano-Martínez, *et al.*, Development and Application of a Lignin-Based Polyol for Sustainable Reactive Polyurethane Adhesives Synthesis, *Polymers*, 2024, **16**(13), 1928.
55 Y. Ou, *et al.*, Investigation on the thermal decomposition of hydroxyl terminated polyether based polyurethanes with inert and energetic plasticisers by DSC-TG-MS-FTIR, *J. Anal. Appl. Pyrolysis*, 2018, **132**, 94–101.
56 J. Mattia and P. Painter, A Comparison of Hydrogen Bonding and Order in a Polyurethane and Poly(urethane–urea) and Their Blends with Poly(ethylene glycol), *Macromolecules*, 2007, **40**(5), 1546–1554.
57 T. Li, *et al.*, Curing kinetics of block copolymerisation thermoset polyurethane by non-isothermal DSC method, *J. Appl. Polym. Sci.*, 2025, **142**(3), e56374.